A quantitative account of electron energy transport in a National Spherical Tokamak Experiment plasma[a)]

K. L. Wong,[a)] S. Kaye, D. R. Mikkelsen, J. A. Krommes, K. Hill, R. Bell, and B. LeBlanc
Plasma Physics Laboratory, Princeton University, Princeton, New Jersey 08543, USA

(Received 9 November 2007; accepted 7 January 2008; published online 4 March 2008)

The first successful quantitative account of the electron thermal conductivity χ_e in a tokamak experiment due to imperfect magnetic surfaces is presented. The unstable spectrum of microtearing instabilities is calculated with the GS2 code for a well-behaved H-mode plasma in the National Spherical Tokamak Experiment [M. Ono *et al.*, Nucl. Fusion **40**, 557 (2000)], with 6 MW deuterium neutral beam heating at $I_p = 0.75$ MA, $B_t = 0.5$ T. The application of existing nonlinear theory shows that the unstable modes can produce overlapping magnetic islands leading to global stochastic magnetic fields. The calculated χ_e based on the present theory is in reasonable agreement with the values from transport analysis of the experimental data over the entire region $(0.4 < r/a < 0.75)$ where the electron temperature gradient is strong enough to make microtearing the most unstable mode. There is no adjustable parameter in this comparison. This instability can be avoided by reversed magnetic shear or by heating the electrons to lower the electron-ion collision frequency.
 [DOI: 10.1063/1.2839295]

I. INTRODUCTION

Anomalous electron transport in magnetized plasmas can be a major obstacle in the way toward practical nuclear fusion power, and it has been an outstanding problem for almost half a century. With the same kinetic energy, the electron velocity is larger than the ion velocity by the factor $(m_i/m_e)^{1/2} \sim 60$ in deuterium plasmas, and the electron gyroradius is smaller than the ion gyroradius by the same factor. Therefore, it should not be a surprise to see that these two plasma species have different transport properties in magnetic fusion confinement devices. Major advances were made in the past two decades in the understanding of ion transport via ITG (ion temperature gradient mode) turbulence. Elimination of ITG turbulence by plasma flow shear has been proven successful in many tokamak experiments where ion energy transport can be reduced to a neoclassical level. However, electron energy transport remains anomalous, and this has become the new frontier in fusion research. Based on the successful experience in ion channel transport, ETG (electron temperature gradient mode) turbulence is the natural suspect responsible for electron energy transport,[1] which may be true in some tokamak experiments.[2,3] Correlations between short-wavelength fluctuations and local electron thermal conductivity were first observed in the TFTR (Tokamak Fusion Test Reactor) tokamak,[4–6] and more recently in the DIII-D tokamak.[7,8] While active theoretical and experimental research continues along this path,[9,10] here we investigate the effect of magnetic field fluctuations on electron energy transport in the NSTX (National Spherical Tokamak Experiment) spherical tokamak (ST).[11]

Due to their small gyroradii and high velocities, electrons move along magnetic field lines just like trains moving on rails; they go wherever the field lines lead them to, and they are very sensitive to small imperfections of magnetic surfaces. The concept of magnetic braiding[12] was first introduced in 1973 to explain anomalous electron transport and other experimental observations in tokamak experiments. Those analyses could not be made quantitative, probably because magnetic braiding occurs only in some small localized regions in tokamaks, i.e., there are plenty of good magnetic surfaces to provide good electron confinement, and the mixture of these regions makes detailed quantitative analysis difficult. It was discovered recently[13] that microtearing instabilities in spherical tokamaks can destroy magnetic surfaces over an extended region in the plasma interior where there is a steep electron temperature gradient to drive and sustain these instabilities. Detailed analyses of the experimental data were carried out, and it was found that the experimentally determined electron thermal conductivity is in reasonable agreement with existing theory.[14,15] To the best of our knowledge, this is the first successful quantitative account of electron energy transport in a tokamak plasma, and the details of this investigation are presented in this paper.

The paper is organized as follows: In Sec. II, we briefly describe how magnetic surfaces in tokamaks are destroyed. Section III presents the electron thermal conductivity in a stochastic magnetic field and how this theory should be applied to a tokamak plasma. Experimental results from NSTX are presented in Sec. IV, where comparison of the local electron thermal conductivity with existing theory is made. Section V outlines several methods of remedy for this problem in spherical tokamaks, and a summary is given in Sec. VI.

II. DESTRUCTION OF MAGNETIC SURFACES

Magnetic plasma confinement relies on good magnetic surfaces,[16,17] which exist in many ideal cases. Nonideal situations such as misalignment of field coils or local plasma current due to plasma instabilities can destroy magnetic sur-

[a)]Paper NI1 4, Bull. Am. Phys. Soc. **52**, 187 (2007).
[a)]Invited speaker.

faces. The trajectory of a magnetic field line is the solution to the field line equation[1]

$$d\boldsymbol{x}/d\tau=\boldsymbol{B}(\boldsymbol{x}). \qquad (1)$$

The trajectory is uniquely determined by the starting point when $\boldsymbol{B}(\boldsymbol{x})$ is a single-valued function of $\boldsymbol{x}$—the spatial coordinate, and τ is the length of the field line. The formation of magnetic islands in toroidal plasma confinement devices was first demonstrated by Kerst[18] in 1962 by numerically integrating Eq. (1); analytic proof for the existence of magnetic islands appeared four years later.[19] Kerst[18] also introduced a simple physical picture to illustrate the concept of resonant perturbation, and showed the equivalence of the field line equation and Hamilton's equations in Cartesian coordinates. Therefore, a field line trajectory is analogous to a particle trajectory in classical mechanics; some properties of magnetic field lines can be obtained without actually solving the field line equation. In magnetic flux coordinates, the Hamiltonian form of the field line equation becomes obvious:[1] The poloidal angle θ takes the place of the generalized momentum p, the toroidal flux Ψ takes the place of the generalized coordinate q, the toroidal angle ϕ takes the place of the time variable t, and the poloidal flux Ψ_p takes the place of the Hamiltonian H. In classical mechanics, a particle trajectory is uniquely determined by its initial conditions, as is the trajectory of a magnetic field line. Although these trajectories are deterministic, they can be exponentially sensitive to the initial conditions. The rapid development of chaos theory in the past few decades has brought about the discovery of many fascinating features of Hamiltonian flow in phase space,[20] making it difficult to invoke the ergodic hypothesis as the basis of statistical mechanics.[21] This field is now a branch of applied mathematics where "chaos," "ergodicity," and "stochasticity" have slightly different meanings. However, in the plasma physics literature, these terms are used interchangeably, and therefore we make no effort to draw the fine distinction here.

Instead of tracing field line trajectories in configuration space, it is far more convenient to investigate the general properties of magnetic surfaces using the standard map,[22] $\theta_n=\theta_{n-1}+\Psi_{n-1}$, $\Psi_n=\Psi_{n-1}+K\sin\theta_n$. Figure 1(a) shows the standard map, which qualitatively represents the flux surfaces of a tokamak in the presence of small nonideal magnetic perturbations. While perfect tokamak flux surfaces are represented by a set of horizontal lines $\Psi=\Psi_i$, nonideal small perturbations produce island structures near the rational surfaces where $q=m/n$ are low-order rational numbers. Island chains of different helicity are separated by KAM (Kolmogorov–Arnold–Moser) surfaces, which serve as electron transport barriers, and stochastic magnetic field lines are localized near the separatrix. During the island growth phase, there is a strong current sheet localized at the island boundary—the resistive layer depicted in Fig. 1(b)—where field line reconnection takes place. At small magnetic perturbation, K is small ($\ll 1$) and the island width is proportional to $K^{1/2}$. One can estimate the island width from $\delta B/B$ and expect the destruction of the KAM surfaces when adjacent islands overlap, i.e., when $\Delta r \leqslant (w_i+w_j)/2$. However, numerical experiments indicate that the KAM surfaces are usually destroyed before islands overlap; it typically happens when $(w_i+w_j)/2 \geqslant 2/3\,\Delta r$, the "two-thirds rule."[23] When the KAM surfaces disappear, the magnetic field lines become globally stochastic; that happens for the standard map when

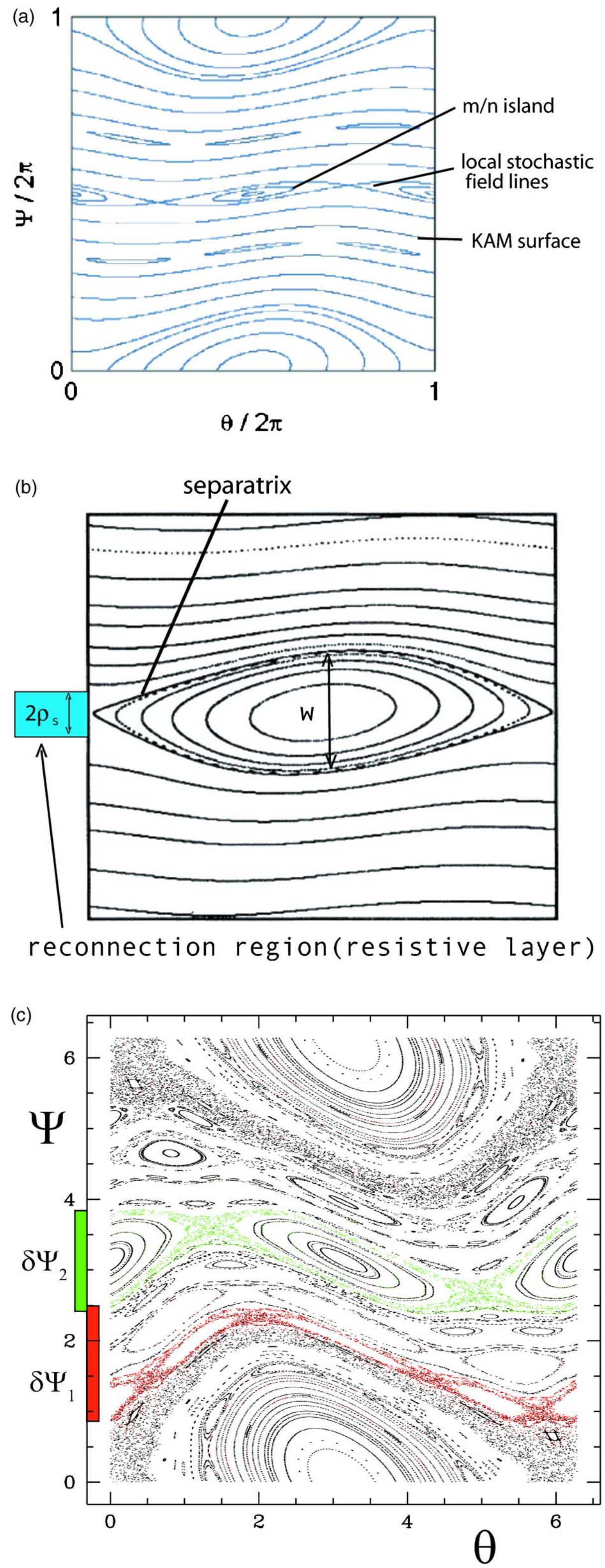

FIG. 1. (Color online) Schematic of magnetic surfaces generated by standard mapping: (a) Magnetic islands separated by KAM surfaces. (b) Resistive layer of a magnetic island. (c) Standard map at $K=0.95$, just before the transition to global stochasticity.

$K > 0.9716\ldots$,[24] where one can find magnetic field lines that cover all values of Ψ as illustrated in Fig. 3 of Ref. 1. Among the stochastic sea of field lines, fractal structures may also be found.[25] Figure 1(c) shows the standard map at $K = 0.95$, just below the threshold value 0.9716…; the "red" field line wanders through the extended region $\delta\Psi_1 = (0.8, 2.5)$ and the "green" field line wanders through $\delta\Psi_2 = (2.4, 3.8)$. This can be viewed as the transition state between local and global stochasticity.

Tearing modes[26] form magnetic islands and change the magnetic field topology in tokamaks. The perturbed magnetic field has a radial component B_r with a jump discontinuity in its radial derivative due to a current sheet of thickness of the order ρ_s within which field line reconnection occurs. Here, ρ_s denotes the ion sound radius $((T_e + T_i)/m_i)^{1/2}/\omega_{ci}$, which is larger than the electron skin depth c/ω_{pe} for the parameters of our interest. This current sheet may be treated as the boundary layer (or resistive layer) of a magnetic island, and one can assume the minimum island width including its boundary is $2\rho_s$. The dynamic evolution of this current sheet is complicated during the growth phase of tearing mode instability; it may start with thickness ρ_s, but then collapses[27–29] into a much thinner layer followed by self-similar generation of secondary islands. This is a subject still under active investigation. Most of these results came from numerical simulations of the $m/n = 1/1$ tearing mode based on reduced magnetohydrodynamic (MHD)[30] or further simplified model equations; they are still pending experimental verification.[31] Putting all these complexities aside, it is not difficult to see that when Δr (the spatial separation between two neighboring island chains) is less than $2\rho_s$, the poloidal magnetic field within this region will be very different from what one would expect from the smoothed safety factor profile $q(r)$.

Let us consider two rational surfaces $q(r_m) = m/n$ and $q(r_{m+1}) = (m+1)/n$ with $m, n \gg 1$. The approximate radial separation between these two surfaces is $\Delta r = 1/(nq')$. Since there are infinite rational surfaces within the interval Δr, we need a truncation scheme to select the low-order rational numbers. Let us only consider n of them, namely, $n' = [n/2] \ldots n \ldots [3n/2]$. For each n', there exists an m' such that $m/n < m'/n' < (m+1)/n$, and the average distance between these surfaces is $\delta r = \Delta r/n = 1/(n^2 q')$. When one assumes that the current sheet has the characteristic thickness of $2\rho_s$, independent of the mode number and the island width, then some island resistive layers will overlap if $\delta r < 2\rho_s$, which yields the resistive layer overlap criterion:[32]

$$m > m_o = q(2q'\rho_s)^{-1/2}, \tag{2}$$

where q' denotes the derivative of q with respect to the minor radius r. Equation (2) is satisfied provided the poloidal mode number m is large enough; this is because the modes are more tightly packed at large m (i.e., smaller δr). The current density in the region where resistive layers overlap is very complicated; the poloidal magnetic field there would be very different from that for an ideal tokamak. It is unlikely that KAM surfaces can exist there, and one would expect a substantial increase in electron transport when resistive layers of adjacent island chains overlap.[32] However, one cannot prove that the magnetic field there is stochastic unless adjacent island chains also overlap. This criterion will be given in Sec. IV.

III. ELECTRON THERMAL CONDUCTIVITY IN STOCHASTIC MAGNETIC FIELD

A rigorous plasma transport theory in a stochastic magnetic field is extremely complicated.[33] However, the electron thermal conductivity χ_e in a stochastic magnetic field can be derived based on a simple quasilinear test particle transport model;[14,15] χ_e is proportional to the magnetic field diffusivity $D_M = R|\delta B/B|^2$. Rechester and Rosenbluth's theory[14] was based on a straight cylinder with no average poloidal magnetic field, i.e., $\langle B_\theta \rangle = 0$ and they use the Kolmogorov length as the magnetic field correlation length L_c. Reference 14 follows a magnetic flux tube in a cylinder via area-preserved mapping. When the field line trajectory is exponentially sensitive to its initial position, the circumference of the flux tube grows exponentially with the axial distance along the cylinder, and the Kolmogorov length is the e-folding length of the flux tube circumference. However, in a tokamak, $\langle B_\theta \rangle$ is much stronger than the fluctuating magnetic field; as pointed out by Kadomtsev[34] and also Krommes *et al.*,[33] the connection length qR should be used as the magnetic field correlation length L_c. Then, the thermal electrons with thermal velocity v_e in the NSTX discharge analyzed below are in the collisional regime, i.e., the electron mean free path λ_{mfp} is shorter than L_c, and the aspect ratio of the tokamak becomes unimportant because the bulk of the electrons encounter collisions before they bounce, i.e., they are not trapped. Because nonlinear gyrokinetic simulations of electromagnetic fluctuations are still in the development stage at the moment, we will rely on Drake's theory[35] for the nonlinear saturation level of the instability. It is important to point out here that this theory is based on a shearless slab model with other simplifications argued to be applicable to conventional tokamaks. The theory has not been checked for spherical tokamaks, where magnetic shear can be strong, nor with nonlinear gyrokinetic simulation. From this theory, we expect the unstable microtearing modes to saturate at the amplitude $\delta B/B \approx \rho_e/L_T$, the ratio of electron gyroradius to the electron temperature scale length. Then the χ_e due to these saturated microtearing modes becomes

$$\chi_e = (\rho_e/L_T)^2 R v_e(\lambda_{\mathrm{mfp}}/L_c) = (\rho_e/L_T)^2 v_e^2/(\nu_{\mathrm{ei}} q), \tag{3}$$

where ν_{ei} is the electron-ion Coulomb collision rate. All the values of the plasma parameters on the right-hand side of Eq. (3) can be obtained from the plasma equilibrium. In the collisionless regime, χ_e would be larger[14] by the factor $\lambda_{\mathrm{mfp}}/L_c$, and one also has to account for the fraction of trapped electrons as well. Besides the trapped electron fraction, there may be other toroidal effects that are not contained in Drake's theory but can quantitatively affect the answer too.

IV. COMPARISON WITH EXPERIMENTAL DATA

NSTX is a spherical tokamak operating with major radius $R = 0.85$ m and minor radius $a = 0.67$ m ($R/a = 1.27$). An H-mode discharge with 6 MW deuterium neutral beam heat-

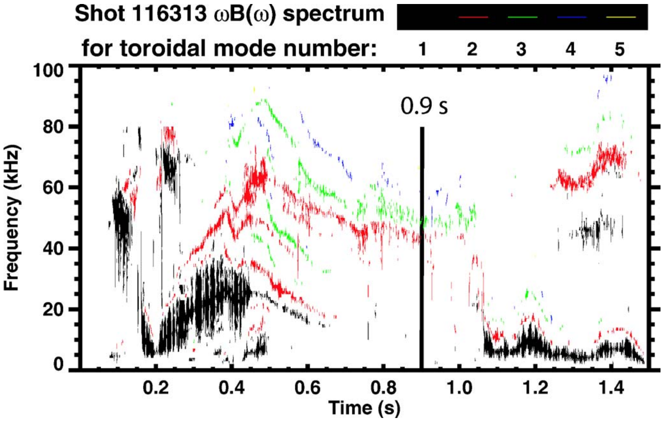

FIG. 2. (Color online) Frequency spectra of the Mirnov coil signal at various toroidal mode numbers n.

ing at $I_p = 0.75$ MA, $B_t = 0.5$ T was chosen for detailed analysis. At $t = 0.9$ s, motional Stark effect measurements of the magnetic field pitch indicate that the plasma has monotonically increasing q with $q(0) > 1$ so that there are no sawteeth or other significant MHD activities in the plasma core observable by the soft-x-ray array or Mirnov coils. The frequency spectrum of the Mirnov coil data is shown in Fig. 2. The smoothed electron temperature, density, and q profiles for this case are depicted in Fig. 3, where the radial location is represented by the square root of the normalized flux, $(\phi/\phi_a)^{1/2} \cong \rho = r/a$. There is a steep temperature gradient at $(\phi/\phi_a)^{1/2} \geqslant 0.4$ where electron confinement is good. The GS2 gyrokinetic stability code[36,37] is used to calculate the linear growth rate and the eigenmode structure for the most unstable mode in a preset range of wave numbers. The input parameters, including the equilibrium, are imported directly from the output file of the TRANSP code.[38] The linear growth rates were calculated for wave numbers in the range $k\rho_s = 0.1$ to 1. Two kinds of unstable modes were found: the ITG mode and the microtearing mode.[39,40] They have distinctly different mode structures: the perturbed electric (magnetic) field has even (odd) parity for ITG, and the parities for the perturbed fields are opposite for microtearing modes, which also have an extended mode structure along the magnetic field. ITG modes propagate in the ion diamagnetic drift direction; the microtearing modes propagate in the electron diamagnetic drift direction, and this is reflected in the negative sign of the real frequency. Microtearing modes are found to be the most unstable mode in the region $(\phi/\phi_a)^{1/2} = 0.4$ to 0.75 of this plasma. Figure 4 shows the linear growth rate of these unstable modes for various wave numbers at $(\phi/\phi_a)^{1/2} = 0.4$, 0.5, 0.65, and 0.75.

Tearing modes require nonzero plasma resistivity to break the magnetic field lines. Microtearing modes are driven by an electron temperature gradient, which usually leads to a pressure gradient that can drive resistive ballooning modes.[41] Therefore, it is important to distinguish these two modes in our experiment. Let us use the standard notation: ω_{*e} is the electron diamagnetic frequency with the electron density scale length L_n, and ω_{*T} is the electron diamagnetic frequency with the electron temperature scale length

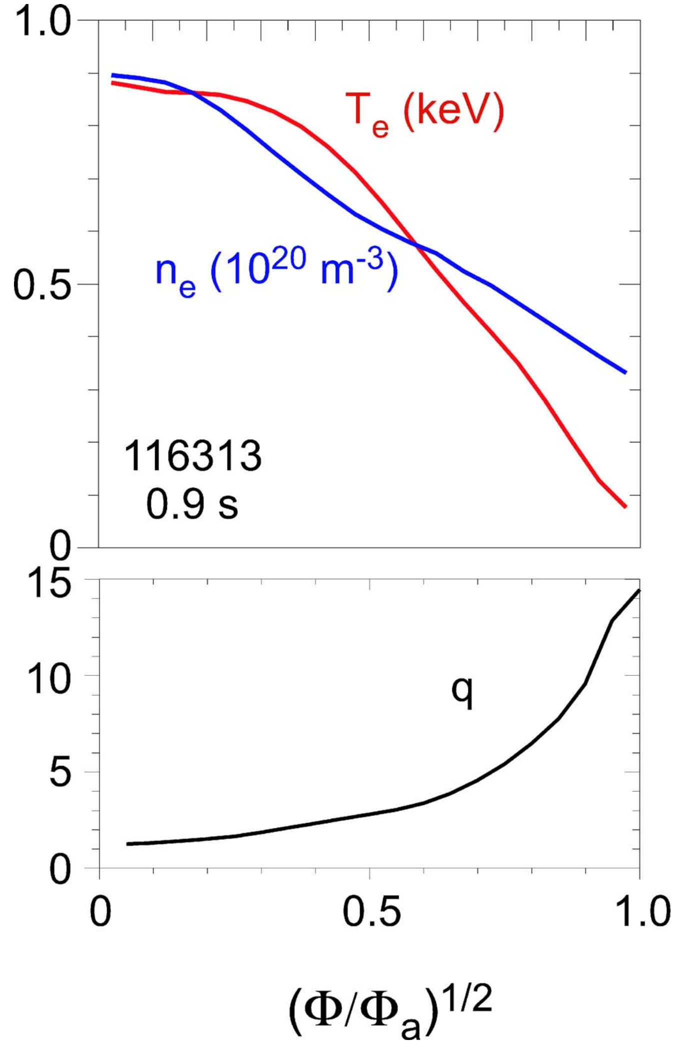

FIG. 3. (Color online) Profiles of electron temperature, electron density, and safety factor for shot 116313.

L_T. The frequency of microtearing mode[42] obeys the dispersion relation

$$\omega = \omega_{*e} + c\omega_{*T}, \quad 0 < c < 1 \tag{4}$$

while the resistive ballooning mode frequency is much lower, $\omega \ll \omega_{*e}$. Let us take the GS2 results at $r/a = 0.5$, where $n_e = 6.5 \times 10^{13}$ cm^{-3}, $T_e = 650$ eV, $L_T = 42$ cm, $L_n = 78$ cm, $B = 5$ kG, and $T_i = 800$ eV. At $k_\theta = 0.9$ cm^{-1}, $\omega = 2.8 \times 10^5$ rad/s, $\omega_{*e} = 1.7 \times 10^5$ rad/s, $\omega_{*T} = 3.1 \times 10^5$ rad/s, and we get $\omega = \omega_{*e} + 0.35\ \omega_{*T}$, i.e., the frequency satisfies the dispersion relation for the microtearing mode, and it is much higher than the expected frequency for the resistive ballooning mode. The calculated unstable spectra for a scan where the electron temperature gradient was manually changed are shown in Fig. 5(a). For $k\rho_s = 0.5$, the instability threshold determined in Fig. 5(b) is at $\eta_e = L_n/L_T \sim 0.5$, which is consistent with the slab model prediction of $\eta_e > 0.3$.[43] In addition, all the unstable microtearing modes from GS2 satisfy the condition $\nu_{ei} > \omega_{*e}$, which is another slab-model prediction.[43] Resistive ballooning modes have larger $k_\parallel$, and their mode structures are strongly peaked at the low-field

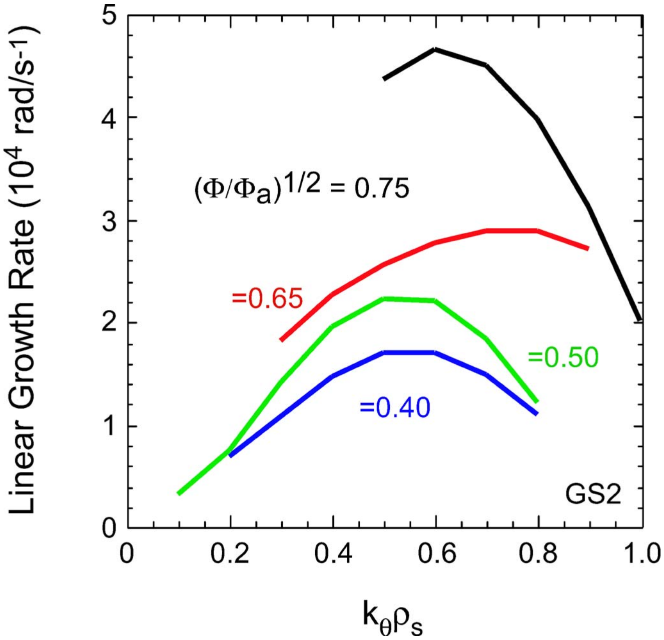

FIG. 4. (Color online) Linear growth rate of unstable microtearing modes at various radial locations ($(\phi/\phi_a)^{1/2} \cong r/a$) in shot no. 116313 at 0.9 s.

side of the tokamak where the bad curvature couples strongly with the pressure gradient. On the contrary, microtearing modes have small $k_\parallel$, so their mode structure is highly elongated along magnetic field lines. When running the GS2 code for microtearing instabilities, we need to use a long flux tube, typically 1.35×10^4 cm long; the corresponding Nyquist wave number is $k_\parallel \sim 2.3\times10^{-4}$ cm$^{-1} \sim 0$, and the parallel mode structure calculated from the GS2 code is indeed elongated. The parallel mode structure for ITG modes is more localized, and the typical length of the flux tube is three times shorter. Based on all the above information, we conclude that these unstable modes we found in NSTX are microtearing and not resistive ballooning modes.

In order to verify that these unstable microtearing modes satisfy the resistive layer overlap criterion, we use Eq. (2) to calculate the values of m_o and $k_o = m_o/r$ at various radial locations ρ, and the results are listed in Table I. Most of the linearly unstable modes shown in Fig. 4 have $k > k_o$, i.e., the resistive layer overlap criterion is well satisfied. In order to check the island overlap criterion, we again rely on Drake's theory[35] for the nonlinear saturation level of the instability, and assume that the unstable modes saturate at the amplitude $\delta B/B \approx \rho_e/L_T$. Since microtearing modes have small $k_\parallel$ and δB has even parity, they are very effective in producing magnetic islands[43] near rational magnetic surfaces where $q = m/n$. The island width can be estimated by the following analytic formula:

TABLE I. Threshold mode number m_o for resistive layer overlap.

$(\phi/\phi_a)^{1/2} \cong r/a$	ρ_s(cm)	m_o	$k_o = m_o/r$ (cm^{-1})
0.4	1.1	6.3	0.24
0.5	1.1	7.2	0.22
0.6	1.0	6.3	0.16
0.7	0.8	6.5	0.14

$$w = 4[b_{mn} R q^2/(m q')]^{1/2}, \tag{5}$$

where $b = \delta B/B$, which can be expressed in terms of the Fourier coefficients b_{mn}. As shown in Sec. II, the separation between adjacent island chains is $\delta r = 1/(n^2 q')$, and they overlap when

$$S = 4m[(m/\Delta m)^{1/2}(m/\delta m q)^{1/2}(R/r)(rq'/q)b]^{1/2} > 1. \tag{6}$$

We can write $b^2 = \Sigma b^2_{mn} = \Delta n\ \delta m\ b^2_{mn}$, where the spectral width $\Delta n = \Delta m/q$ should be much larger than 1, and $\delta m = \Delta k_\parallel/(Rq)^{-1} \geqslant 1$ measures the spread in $k_\parallel$. The saturated island width is obtained by putting the mode amplitude $\delta B/B \approx \rho_e/L_T$. Let us choose the plasma parameters at $r/a = 0.5$, where $q = 2.8$, and put $\Delta m = 20$, $\delta m = 1$, $\delta B/B \approx \rho_e/L_T \sim 3\times10^{-4}$. Then we find that the saturated island width is about $2\rho_s$, not much different from the resistive layer thickness, and $S \geqslant 2$. When we put $\delta m = 2$, we get $w \sim \rho_s$ and $S \geqslant 1$. Based on these numbers, the adjacent island chains due to those unstable microtearing modes in shot 116313 should overlap and the KAM surfaces are destroyed even without

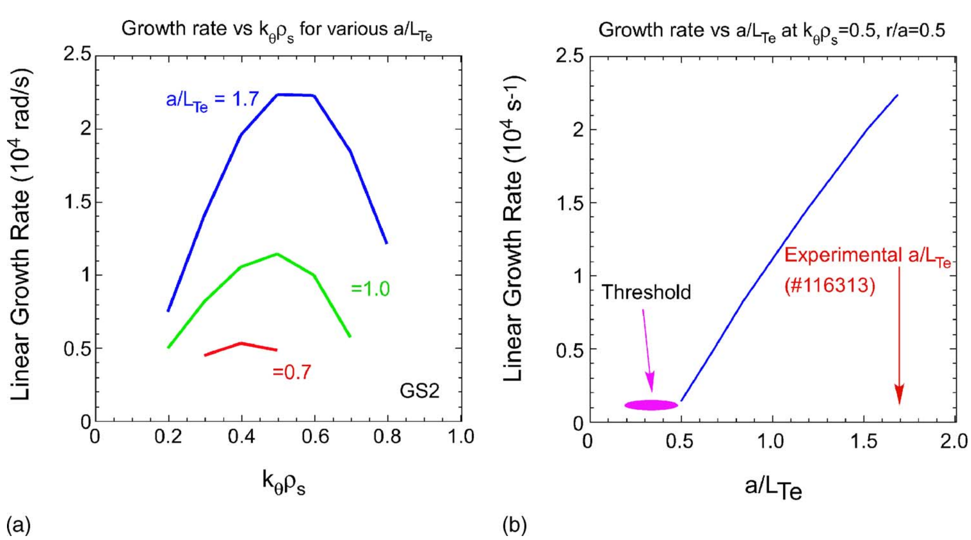

FIG. 5. (Color online) GS2 results with various electron temperature gradients at $r/a = 0.5$. (a) Unstable microtearing mode spectra. (b) Determination of instability threshold at $k\rho_s = 0.5$.

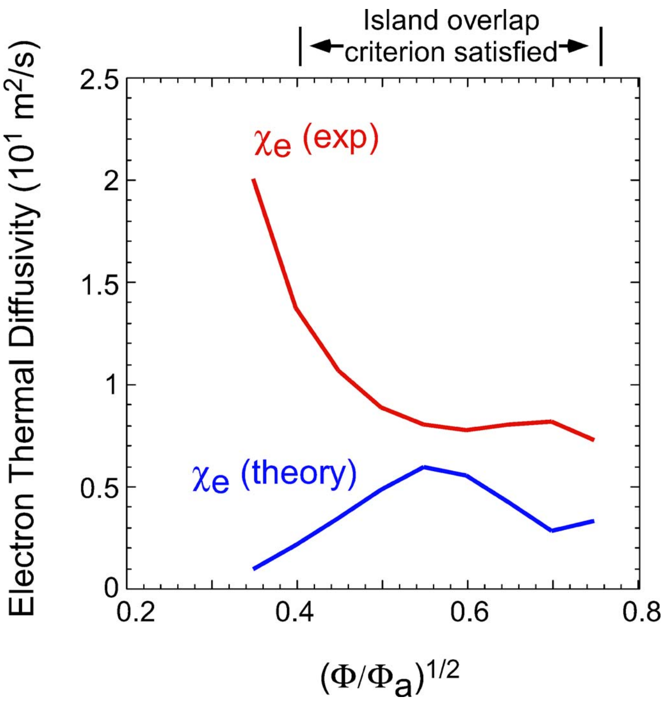

FIG. 6. (Color online) Comparison between values of electron thermal conductivity from TRANSP analysis of the experimental data for shot no. 116313 and those calculated from Eq. (3).

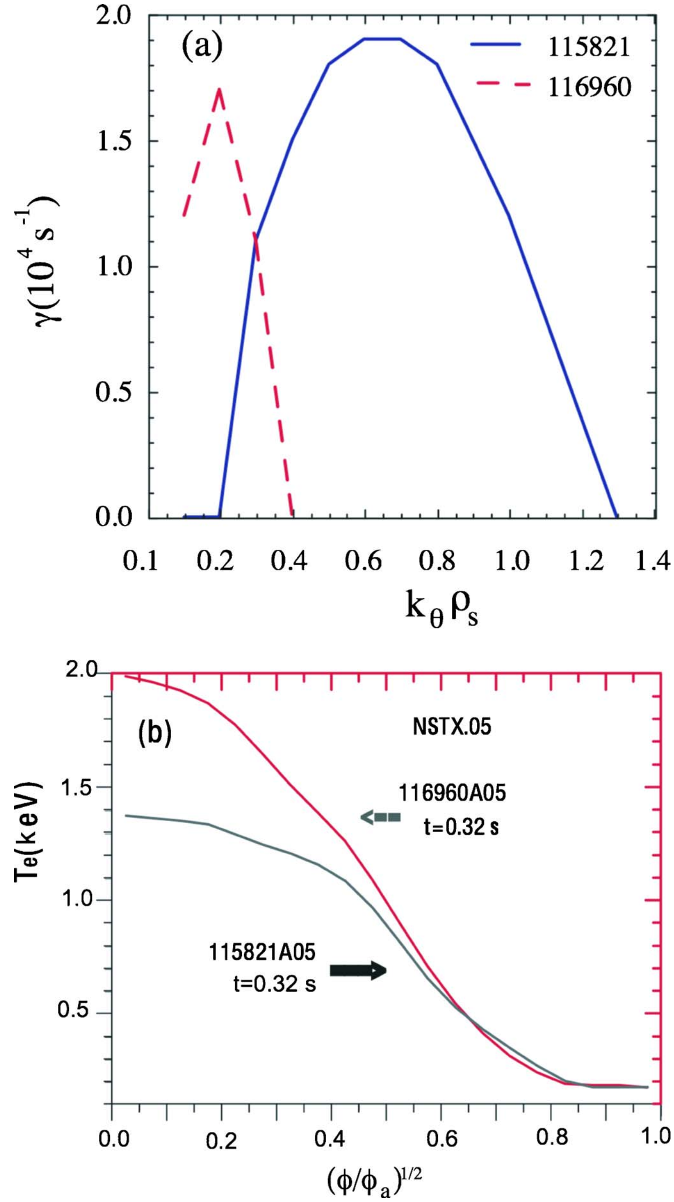

FIG. 7. (Color online) Effects of reversed magnetic shear. (a) GS2 calculation shows that microtearing modes with high k_θ are unstable at $(\phi/\phi_a)^{1/2}=0.3$ in shot no. 115821 but are stable in shot no. 116960, where the magnetic shear is reversed. (b) The central electron temperature is substantially higher in shot no. 116960 when microtearing modes with high k_θ are stable.

invoking the two-thirds rule. Therefore, the region $0.4 \leq (\phi/\phi_a)^{1/2} \leq 0.75$ should be occupied by stochastic magnetic field lines, and Eq. (3) is applicable. These theoretical values are compared to the χ_e obtained from transport analysis with the TRANSP code. The theoretical values are roughly a factor of 2 lower as shown in Fig. 6. Such agreement is satisfactory when one considers the uncertainties associated with the nonlinear theory[35] and the transport analysis of the experimental data.

It is well known today that a toroidal plasma is a very complex object. Different things can happen in different discharges; even in the same discharge, different things can happen in different regions of the plasma. The total energy flux transported through the electron channel is the sum of those for all different mechanisms. We just show that in the region $0.4 < r/a < 0.75$ of shot 116313, electron energy transport due to microtearing modes is the dominant term. Near the magnetic axis where $(\phi/\phi_a)^{1/2} \leq 0.3$, $T_e(r)$ is very flat, and microtearing modes are stable; χ_e there is very large due to other mechanisms not yet identified.

Should microtearing modes be the dominant electron transport mechanism, χ_e will be significantly reduced when these modes are stable, which is the case in a plasma with reversed central magnetic shear.[44] Figure 7(a) shows the linear growth rate at $(\phi/\phi_a)^{1/2}=0.3$ for such a shot (no. 116960) and its comparison shot (no. 115821). Microtearing modes are unstable in no. 115821 over a wide range of $k_\theta \rho_s$, but are unstable over a much narrower range in no. 116960 where the magnetic shear is reversed. The unstable modes in no. 116960 have low mode number and do not satisfy the overlap criterion. Both shots have the same plasma current, density, magnetic field, plasma shape, position, and neutral beam heating power. As depicted in Fig. 7(b), the central electron temperature is substantially higher (2 keV vs 1.4 keV) in no. 116960 where microtearing modes are stable. This is a strong indication that microtearing modes may be the dominant mechanism responsible for the electron transport at this location in this type of plasma. At present, however, there is no diagnostic on NSTX capable of measuring the internal magnetic field fluctuations to confirm the existence of microtearing modes.

V. POSSIBLE REMEDIES

Reversed magnetic shear is one possible way to avoid microtearing instabilities as shown above. Another possibility is to lower the electron collision frequency. Starting with

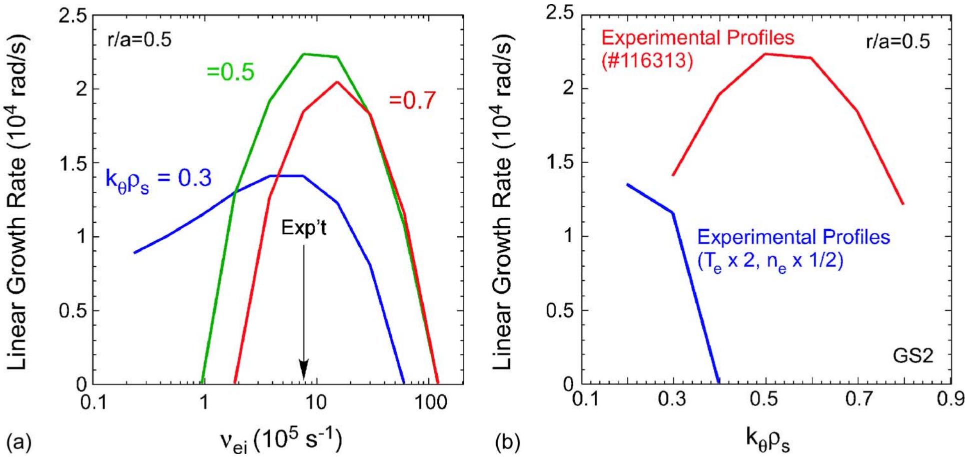

FIG. 8. (Color online) The effect of electron collision frequency on microtearing instability. (a) Dependence of the linear growth rate of microtearing instability on electron collision frequency (log-scale) at various wave numbers. The arrow marks the experimental value at $\nu_{ei}=8\times10^5$ s^{-1}. (b) Stabilization of high k_θ microtearing instabilities in NSTX by doubling T_e and reducing n_e by half.

the plasma parameters of shot no. 116313 at $r/a=0.5$, we perform a scan changing the electron collision frequency ν_{ei}. The calculated instability growth rates are depicted in Fig. 8(a) as a function of ν_{ei}. It is apparent that the experimental condition for shot no. 116313 marked by the vertical arrow labeled "Exp't" is sitting near the peak of the growth rate for the microtearing instability. The low-*m* modes are less sensitive to ν_{ei}, but those high-*m* modes responsible for producing stochastic magnetic field via island overlap can be stabilized by reducing ν_{ei}. In fact, this is the reason that in the interior of present large tokamaks, microtearing modes are stable[45–47] because they operate at lower densities and higher temperatures compared with spherical tokamaks. To demonstrate that this scenario can actually work for NSTX, we modify the plasma parameters at $r/a=0.5$ of shot no. 116313 by changing n_e to $n_e/2$, T_e to $2T_e$ (i.e., β_e remains the same); the GS2 calculations show that the high-*m* modes are indeed stable as shown in Fig. 8(b).

Should it become too difficult to stabilize the microtearing instability, one can always raise the magnetic field to lower the saturation amplitude down to a tolerable level and avoid island overlap. Magnetic islands are present in many tokamak discharges; they cannot do much harm as long as the stochastic magnetic field is localized within a small region in the plasma.

VI. SUMMARY

In a well-behaved NSTX beam heated H-mode plasma, confinement is good in the region $0.4<r/a<0.75$ where a steep electron temperature gradient can be sustained, and microtearing modes are found to be unstable there. Existing nonlinear theory indicates that these unstable modes should saturate at amplitudes high enough to produce globally stochastic magnetic field due to magnetic island overlap. The experimentally observed electron thermal conductivity in this region is in good agreement with that calculated from Eq. (3). This should not be a surprise because all the assumptions based on which Eq. (3) is derived are true. This instability could be the most likely limit[48] on electron temperature in STs where the intrinsic high $\boldsymbol{E}\times\boldsymbol{B}$ shears can stabilize the usual long-wavelength instabilities. However, NSTX has the flexibility to operate in many regimes, and the microtearing instability is not an intrinsic property of STs. It turns out this way in this plasma primarily because of the high density and low electron temperature. This instability could be suppressed by reversed magnetic shear, by raising the electron temperature such that $\nu_{ei}<\omega_{*e}$, or by operating at higher magnetic field to reduce the saturation amplitude. This result does not rule out ETG turbulence in controlling electron transport in NSTX. In fact, ETG modes are calculated to be important in other discharges and/or at other locations. This paper neglects the complexities associated with the evolution dynamics of the magnetic fluctuations. Hopefully, they can be treated when the GEM code[49] becomes available in the near future.

ACKNOWLEDGMENTS

We are greatly indebted to Dr. M. G. Bell, Dr. A. L. Roquemore, and all the technical staff of the NSTX group, whose hard work made this experiment possible. We are grateful to Dr. R. B. White for providing the standard map at $K=0.95$, and to Dr. T. S. Hahm and Dr. S. R. Hudson for some useful information. This work is supported by DOE Contract No. DE-AC02-76CH03073.

[1] A. H. Boozer, Rev. Mod. Phys. **76**, 1071 (2004), and references therein.
[2] W. Horton, Rev. Mod. Phys. **71**, 735 (1999).
[3] G. T. Hoang, C. Bourdelle, X. Garbet, G. Giruzzi, T. Aniel, M. Ottaviani, W. Horton, P. Zhu, and R. V. Budny, Phys. Rev. Lett. **87**, 125001 (2001).
[4] R. J. Hawryluk, Rev. Mod. Phys. **70**, 537 (1998).
[5] K. L. Wong, N. Bretz, T. S. Hahm, and E. Synakowski, Phys. Lett. A **236**, 339 (1997).
[6] K. L. Wong, K. Itoh, S.-I. Itoh, A. Fukuyama, and M. Yagi, Phys. Lett. A **276**, 281 (2000).
[7] J. L. Luxon, Nucl. Fusion **42**, 614 (2002).
[8] K. L. Wong, R. V. Budny, R. Nazikian, W. A. Peebles, T. L. Rhodes, R. Prater, C. C. Petty, and R. J. Jayakumar, Bull. Am. Phys. Soc. **50**, 274 (2005).
[9] T. Rhodes, Bull. Am. Phys. Soc. **51**, 335 (2006).
[10] E. Mazzucato, R. E. Bell, J. C. Hosea, B. P. LeBlanc, H. K. Park, D. R. Smith, and J. R. Wilson, Bull. Am. Phys. Soc. **52**, 61 (2007).
[11] M. Ono, S. M. Kaye, Y.-K. M. Peng *et al.*, Nucl. Fusion **40**, 557 (2000).
[12] T. H. Stix, Phys. Rev. Lett. **30**, 833 (1973).
[13] K. L. Wong, S. Kaye, D. Mikkelsen, J. A. Krommes, K. Hill, R. Bell, and B. LeBlanc, Phys. Rev. Lett. **99**, 135003 (2007).
[14] A. B. Rechester and M. N. Rosenbluth, Phys. Rev. Lett. **40**, 38 (1978).
[15] T. H. Stix, Nucl. Fusion **18**, 353 (1978).

[16] L. Spitzer, Jr., Phys. Fluids **1**, 253 (1958).
[17] M. D. Kruskal and R. M. Kulsrud, Phys. Fluids **1**, 265 (1958).
[18] D. W. Kerst, J. Nucl. Energy, Part C **4**, 253 (1962).
[19] M. N. Rosenbluth, R. V. Sagdeev, and J. B. Taylor, Nucl. Fusion **6**, 297 (1966).
[20] D. K. Arrowsmith and C. M. Place, *An Introduction to Dynamical Systems* (Cambridge University Press, Cambridge, UK, 1990), p. 42.
[21] R. Balescu, *Equilibrium and Non-equilibrium Statistical Mechanics* (Wiley, New York, 1975), p. 695.
[22] B. V. Chirikov, Phys. Rep. **53**, 263 (1979).
[23] A. J. Lichtenberg and M. A. Lieberman, *Regular and Chaotic Dynamics*, 2nd ed. (Springer, New York, 1992), p. 250.
[24] J. M. Greene, J. Math. Phys. **20**, 1183 (1979).
[25] J. D. Meiss, Rev. Mod. Phys. **64**, 795 (1992).
[26] H. P. Furth, J. Killeen, and M. N. Rosenbluth, Phys. Fluids **6**, 459 (1963).
[27] M. Ottaviani and F. Porcelli, Phys. Rev. Lett. **71**, 3802 (1993).
[28] D. Borgogno, D. Grasso, F. Porcelli, F. Califano, F. Pegoraro, and D. Farina, Phys. Plasmas **12**, 032309 (2005).
[29] D. Grasso, D. Borgogno, and F. Pegoraro, Phys. Plasmas **14**, 055703 (2007).
[30] F. Porcelli, Phys. Rev. Lett. **66**, 425 (1991).
[31] M. Yamada (private communication).
[32] D. A. D'Ippolito, Y. C. Lee, and J. F. Drake, Phys. Fluids **23**, 771 (1980).
[33] J. A. Krommes, C. Oberman, and R. G. Kleva, J. Plasma Phys. **30**, 11 (1983).
[34] B. B. Kadomtsev and O. P. Pogutse, in *Proceedings of the 7th International Conference on Plasma Physics and Controlled Fusion*, Innsbruck, 1978 (IAEA, Vienna, 1979), Vol. I, p. 649.
[35] J. F. Drake, N. T. Gladd, C. S. Liu, and C. L. Chang, Phys. Rev. Lett. **44**, 994 (1980).
[36] M. Kotschenreuther, G. Rewoldt, and W. M. Tang, Comput. Phys. Commun. **88**, 128 (1995).
[37] W. Dorland, F. Jenko, M. Kotschenreuther, and B. N. Rogers, Phys. Rev. Lett. **85**, 5579 (2000).
[38] R. J. Hawryluk, in *Proceedings of the Course in Physics of Plasmas Close to Thermonuclear Conditions, Varenna, 1979*, edited by B. Coppi *et al.* (CEC, Brussels, 1980), Vol. 1, p. 19.
[39] M. H. Redi, W. Dorland, R. Bell *et al.*, in *Proceedings of the 30th EPS Conference*, edited by R. Koch and S. Lebedev (EPS, Mulhouse, 2003).
[40] D. J. Applegate, C. M. Roach, S. C. Cowley, W. D. Dorland, N. Joiner, R. J. Akers, N. J. Conway, A. R. Field, A. Patel, M. Valovic, and M. J. Walsh, Phys. Plasmas **11**, 5085 (2004).
[41] B. A. Carreras, P. H. Diamond, M. Murakami *et al.*, Phys. Rev. Lett. **50**, 503 (1983).
[42] N. T. Gladd, J. F. Drake, C. L. Chang, and C. S. Liu, Phys. Fluids **23**, 1182 (1980).
[43] J. A. Wesson, *Tokamaks*, 1st ed. (Oxford University Press, New York, 1987), pp. 199.
[44] F. M. Levinton, H. Yuh, M. G. Bell *et al.*, Phys. Plasmas **14**, 056119 (2007).
[45] J. W. Connor, S. C. Cowley, and R. J. Hastie, Plasma Phys. Controlled Fusion **32**, 799 (1990).
[46] N. Ohyabu, G. L. Jahns, R. D. Stambaugh, and E. J. Strait, Phys. Rev. Lett. **58**, 120 (1987).
[47] J. Kesner and S. Migliuolo, Nucl. Fusion **39**, 163 (1999).
[48] M. Kotschenreuther, W. Dorland, Q. P. Liu, M. C. Zarnstorff, R. L. Miller, and Y. R. Lin-Liu, Nucl. Fusion **40**, 677 (2000).
[49] G. Rewoldt, W. M. Tang, Y. Chen, and S. E. Parker, Bull. Am. Phys. Soc. **51**, 320 (2006).